Impact of in-plane disorders on the thermal conductivity of $AgCrSe_2$

Shota Izumi,[1] Yui Ishii,[2,*] Jinfeng Zhu,[3] Tsunemasa Sakamoto,[1]
Shintaro Kobayashi,[4] Shogo Kawaguchi,[4] Jie Ma,[3] and Shigeo Mori[1]

[1] *Department of Materials Science, Osaka Metropolitan University, Osaka 599-8531, Japan*
[2] *Co-Creation Institute for Advanced Materials, Shimane University, Shimane 690-8504, Japan*
[3] *School of Physics and Astronomy, Shanghai Jiao Tong University, Shanghai 200240, China*
[4] *Japan Synchrotron Radiation Research Institute (JASRI), Hyogo 679-5198, Japan*

Superionic conductors have recently attracted renewed attention for their use as thermoelectric materials due to their extremely low lattice thermal conductivity. Of central interest is why the superionic conductors exhibit such low thermal conductivity, and competing mechanisms have been proposed thus far. In this study, we investigate the effects of Cu and Au substitution for Ag site on the crystal structure and thermal properties of $AgCrSe_2$, which exhibits superionic conduction of Ag ions. We show that Au substitution significantly reduces the lattice thermal conductivity of $AgCrSe_2$. Powder structure analysis using synchrotron x-ray diffraction reveals that Au substitution increases the anisotropic atomic displacement parameter of Ag ions along the a and b axes. This result indicates that the amplitude of in-plane vibrations is enhanced, which is attributed to increased anharmonicity in the potential energy around Ag ions. The enhanced vibrational amplitude also suggests a reduction in the force constants between Ag ions. Consequently, the enhanced anharmonicity not only shortens the phonon lifetime (τ) by increasing phonon-phonon scattering, but also increases the number of low-energy phonons, which further contributes to the reduction of τ. This anharmonicity mechanism is applicable to other superionic conductors exhibiting ultra-low thermal conductivity, promoting their widespread use as thermoelectric materials.

I. INTRODUCTION

Materials with superionic conductivity often exhibit extremely low thermal conductivity (κ) and are therefore expected to be used as high-performance thermoelectric materials. For example, Cu_2Se, MCrSe$_2$ (M = Ag and Cu), and Ag_8SnSe_6 are the superionic conductors that have been known to exhibit extremely low κ of 0.1∼1 W K^{-1} m^{-1} at 300 K [1–4]. In order to promote the widespread use of thermoelectric conversion materials, it is desirable to clarify the mechanism behind the low κ of these materials, and several competing mechanisms have been proposed thus far [3–10].

One explanation is the liquid-like ionic diffusion that directly scatters phonons, which has been first mentioned in Cu_2Se[3]. On the other hand, several reports have proposed lattice anharmonicity mechanisms [4–7]. For example, in Ag_8SnSe_6, where Se ions are responsible for ionic conduction, diffusive properties in the lattice dynamics have recently been reported, and anharmonic vibration of the Se ions has been pointed out to be essential for realizing the extremely low lattice thermal conductivity [4]. The importance of the lattice anharmonicity has also been emphasized in Mg_3Bi_2 [8]. Localized vibrations of the conducting ions in quasi-2D potential wells have also been proposed [10]. However, these proposed mechanisms have been highly controversial, and the nature of anharmonicity as well as its microscopic mechanism on phonon scattering remain unclear. It is indispensable to focus on a system that allows systematic tuning of the chemical composition and to clarify how the conducting ions affect the thermal conductivity.

In general, the physical properties associated with phonons are often obscured at high temperatures due to the large number of thermally populated phonons, many of which are not directly related to the properties of interest. Particularly, the majority of lattice thermal conductivity is owed to long-wavelength acoustic phonons. Therefore, it is crucial to know the low-temperature properties to discuss the thermal transport by phonons. Nevertheless, most studies on thermoelectric materials with superionic character concentrate on the high-temperature properties of the superionic phase, and the reports on the low-temperature behavior are limited. Recently, inelastic neutron scattering on Ag_8SnSe_6 has revealed that the phonon spectrum of the material is unusually broadened already at several 10 K, which is much lower than the temperature the superionic conduction occurs [4]. This fact implies that a characteristic lattice vibration with very high anharmonicity exists in the superionic conductors, and simultaneously, the low-temperature behavior includes essential information to understand the thermal properties of these materials. Broadening of the phonon signal far below the transition has also been observed in $AgCrSe_2$ [10], although the details have not been mentioned.

Here, we focus on the layered chromium selenides MCrSe$_2$ (M = Cu and Ag) and their possibility of introducing atomic disorder to the superionic species. The reported thermal conductivity at room temperature is ∼0.8 and 0.4 W K^{-1} m^{-1} for M = Cu and Ag, respectively [10–14]. At high temperatures, they crystallize in a rhombohedral structure (a space group $R\bar{3}m$) with face-sharing $CrSe_6$ octahedral layers stacked along the c-axis

* yishii@mat.shimane-u.ac.jp

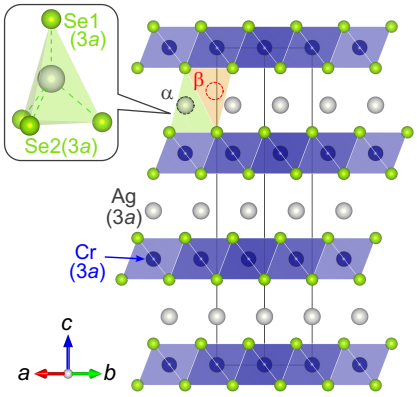

FIG. 1. Crystal structure of the low-temperature phase of $AgCrSe_2$ (a space group $R3m$). The crystal structures throughout this paper are all visualized using VESTA [21]. There are two tetrahedral seats for Ag atoms, as indicated by α and β, one of which is preferentially occupied at temperatures below the $T_{\rm od}$.

direction of the trigonal cell. The succession of the $CrSe_6$ layers forms elongated tetrahedral sites with equivalent two seats, which are indicated as α and β in Fig. 1. The M ions expediently occupy the two seats at a ratio of 1:1 [15] but are delocalized and mobile by hopping between them, resulting in the superionic conduction. The structure undergoes an order-disorder transition for the occupancy of M ions at 365 and 475 K for $CuCrSe_2$ and $AgCrSe_2$, respectively, below which one of the seats is preferentially occupied [11, 16, 17]. Consequently, the inversion center is broken, and the crystal transforms into the low-temperature structure of a space group $R3m$. This transition accompanies a sharp jump in the specific heat and a discontinuity in the lattice constant [17–20], indicating that the transition is of the first-order character.

Several attempts have been made to clarify the extremely low thermal conductivity of this system, and the proposed mechanisms include the localized vibrations by quasi-2D potential [10], and the strong anharmonicity [6]. According to phonon calculations and inelastic neutron scattering, $CuCrSe_2$ and $AgCrSe_2$ possess transverse acoustic (TA) branches with flat dispersions exhibiting a density-of-states (DOS) peak at 8 and 4 meV, respectively [6, 18, 20]. Site-projected DOS calculations have revealed that the TA modes are characterized as the in-plane vibration of the conducting Cu and Ag ions. It should be noted that the energy of the DOS peak of $AgCrSe_2$ is approximately half of that of $CuCrSe_2$. Here, the thermal conductivity of $AgCrSe_2$ is also approximately half of that observed in $CuCrSe_2$ at room temperature. This coincidence implies that the in-plane vibration of Ag and Cu ions is crucial for the low thermal conductivity in this system. The flat dispersions across the k-space should generate highly localized vibrations owing to the very low group velocities and have also been believed to contribute to the ultralow $\kappa_{\rm lat}$ [6].

On the other hand, the longitudinal acoustic (LA) branch has been characterized as the vibration along the c axis and exhibits the DOS peak at 12 and 10 meV for M = Cu and Ag, respectively. These longitudinal vibrations have also been discussed as the candidate: inelastic neutron scattering (INS) experiments using $AgCrSe_2$ powder have reported that the LA mode survives even at high temperatures above the order-disorder transition temperature ($T_{\rm od}$), and in contrast, the TA modes are damped entirely by the diffusive Ag ions [20]. Based on these results, the authors conclude that the robust LA mode causes the "liquid-like" low thermal conductivity. However, another INS experiment argues that the TA modes do coexist with the Ag diffusion in the superionic phase [6].

From the structural viewpoint, the anisotropic displacement parameter U_{11} for the M site has been reported to be an order of magnitude larger than U_{33} in $AgCrSe_2$ [20]. The highly anisotropic displacement parameters have also been reported in $AgCrS_2$ [22–24]. These anisotropic values are attributed to the amplitudes of the in-plane and out-of-plane vibrations of the M atoms, respectively. In addition, the reported value of U_{11} for $AgCrSe_2$ is approximately 0.1 Å^2 at room temperature, which is larger than that for $CuCrSe_2$ by a factor of two [17, 20]. These facts raise questions if the magnitude of U_{11} itself is important in reducing κ or if other factors such as anharmonicity have a major contribution. In addition, it has been reported that the U_{11} of the Ag ions maintains a large value even at 4 K [15], suggesting that the in-plane vibration of Ag ions may be preserved down to near the absolute zero temperature. Based on these backgrounds, we aim to clarify the role of the Ag-site disorder on thermal conductivity by applying atomic substitution of 11$^{\rm th}$ group elements, Cu and Au, for the Ag site.

II. EXPERIMENTAL

Powder samples of $Ag_{1-x}M_xCrSe_2$ (M = Cu and Au) were synthesized using a conventional solid-state reaction. Ag (Rare Metallic, 99.9%, powder), Cu (Rare Metallic, 99.9%, powder), Au (Nilaco, 99.99%, powder), Cr (Rare Metallic, 99.9%, powder), and Se (Kojundo Chemical Laboratory, 99.9%, powder) were mixed at a molar ratio of 1-x : x : 1 : 2, uni-axially pressed into a pellet, and then put in an evacuated silica tube. Before mixing, Cu powder was heated at 200°C for one hour in flowing H_2 gas to reduce copper oxides. The tube was first heated to 200°C in one hour and kept for 6 hours. The tube temperature was raised to 900°C at a ratio of 350°C/h, kept for 24 hours, and then cooled in a furnace at a ratio of approximately 150°C/h. Sample purity was confirmed using a laboratory x-ray diffraction (Cu-Kα) prior to the physical property measurements. Differential scanning calorimetry (DSC) was performed to determine

the T_{od}. Samples for physical property measurements were prepared as follows. The powder sample was uniaxially pressed into a pellet, pressed again in hydrostatic pressure, put in an evacuated silica tube, and then sintered at 900°C for 20 hours. Samples were cut into a rectangular shape for thermal conductivity, electrical resistivity, and specific heat measurements.

Electrical resistivity and specific heat were measured using a four-probe method and the relaxation method, respectively, in a physical property measurement system (PPMS, Quantum Design). Thermal conductivity was measured using the steady-state method in the PPMS, with a commercial sample holder. The values of the cold and hot thermometers were read by the built-in instruments in the PPMS, and the heater power was controlled using external devices connected to the heater terminals. Synchrotron x-ray diffraction was performed at the BL02B2 and BL19B2 beamlines at SPring-8.

III. RESULTS AND DISCUSSION

Figs. S1(a) and S1(b) [25] display the powder x-ray diffraction patterns for M = Cu and Au ($x \leq 0.05$), respectively, obtained using the laboratory x-ray diffractometer. While the samples remain in a single phase up to $x = 0.03$, a secondary phase of Ag_2Se or Se appears at compositions of $x \geq 0.04$ and $x = 0.05$ for M = Cu and Au, respectively. These secondary phases can occur independently of Cu or Au addition and are not due to an excess amount of substitution. However, their occurrence is minimized as much as possible.

Fig. 2(a) shows the synchrotron x-ray diffraction (sXRD) patterns of $AgCrSe_2$ and $Ag_{0.97}M_{0.03}CrSe_2$ (M = Cu and Au) measured at room temperature. Samples used for the synchrotron experiments were different from those shown in Fig. S1 and include a small amount of the secondary phase. In addition, they were prepared by carefully gathering a very small amount of originally fine crystal grains, which were obtained without grinding the sample after reaction, and placing them in a capillary with a diameter of 0.2 mm. The lattice constants obtained from the sXRD are summarized in Fig. 2(b). The lattice constant a is insensitive both for Cu and Au addition and shows an almost constant value. The lattice constant c varies systematically depending on the ionic size of the M site atom, indicating the successful substitution of these elements for the Ag site.

Fig. 3(a) shows the DSC curves of $x = 0$ sample obtained during heating and cooling procedures. A peak is observed in each curve approximately at 480 K, indicating the order-disorder transition of Ag ions. Because the peak positions slightly differ from each other due to the first-order nature of the structural phase transition, the T_{od} is defined as the midpoint between the peak positions observed in the two curves. T_{od} of $x = 0$ determined in this way is 479 K, which agrees well with the reported value [16].

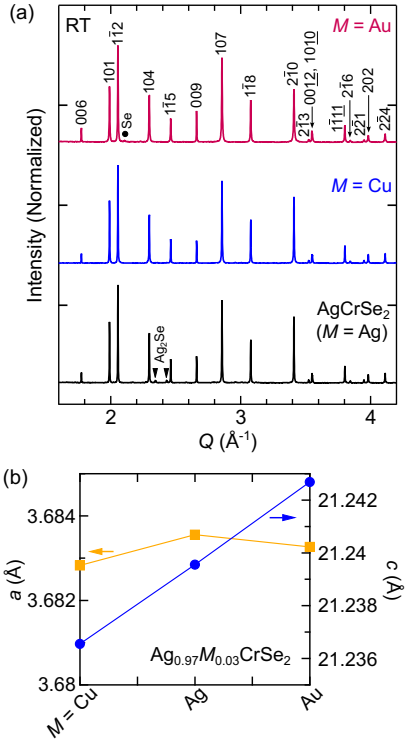

FIG. 2. (a) Synchrotron x-ray diffraction patterns of $AgCrSe_2$ and $Ag_{0.97}M_{0.03}CrSe_2$ (M = Cu, Au) powders obtained at room temperature. Data were collected at the BL19B2 beamline. The incident x-ray energy is set at 24 keV, and the calibrated wavelength λ is 0.51689 Å. Filled triangles indicate Ag_2Se, and a filled circle represents Se as secondary phases. (b) Lattice constants a and c obtained from the diffraction patterns. The error bars are within the range of the marker size.

Figs. 3(b) and 3(c) represent the DSC curves for M = Cu and Au, respectively, obtained during a heating procedure. All the DSC data, including cooling procedures, are presented in Fig. S4 [25]. Fig. 3(d) shows the determined T_{od} plotted as a function of x. The T_{od} systematically decreases with increasing the substitution levels of Cu and Au up to $x = 0.03$. Further decrease in the T_{od} is not observed at $x = 0.04$ both for Cu and Au, indicating that the solid solubility limit is approximately at $x = 0.03$ for both elements. The decrease in the T_{od} by Au substitution is also confirmed using synchrotron x-ray diffraction with varying temperatures, as shown in Figs. S2 and S3 [25]. Figs. S5(a) and S5(b) [25] show the DSC curves of heating and cooling procedures, respectively, obtained using another series of the Cu-substituted samples from those plotted in Fig. 3(b). The T_{od} determined from these curves are compared in Fig. S5(c) with the samples described above. The x variation of T_{od} shows a good reproducibility, as shown in Fig. S5(c), and the uncertainty in the T_{od} is found to be approximately 1 K.

The decrease in the transition temperature indicates that the structure of the low-temperature phase becomes

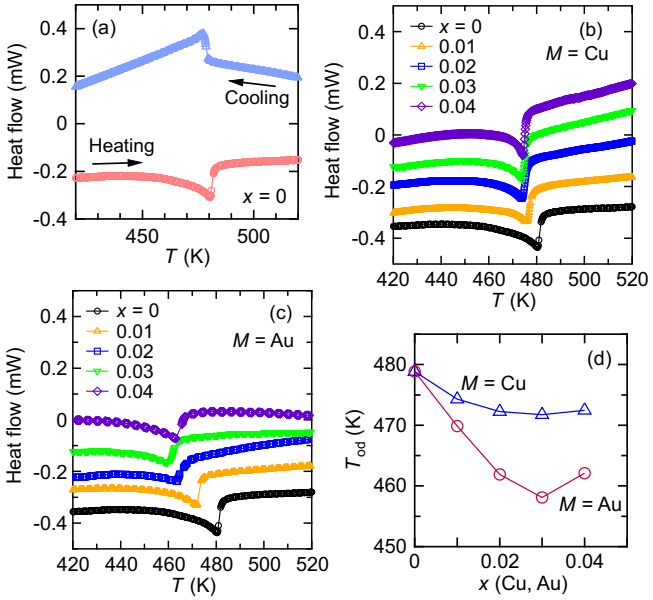

FIG. 3. (a) DSC curves of $x = 0$ obtained during heating and cooling procedures. Because of the first-order character of the order-disorder structural phase transition, there is a small difference between the peak positions of the two curves. (b) and (c) show the DSC curves of M = Cu and Au powder samples, respectively, in a chemical formula $Ag_{1-x}M_xCrSe_2$. The curves were obtained during a heating procedure at a rate of 10 K / min. Data are offset vertically for clarity. (d) T_{od} of $Ag_{1-x}M_xCrSe_2$ (M = Cu and Au) powder samples. The T_{od} was determined as a midpoint of the peak temperatures of the heating and cooling curves.

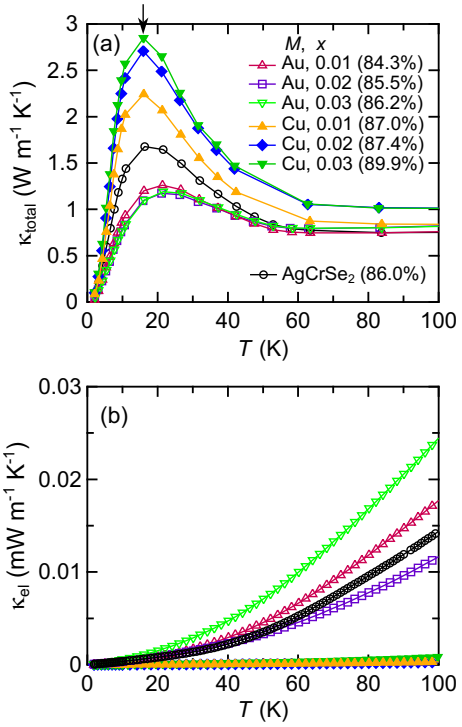

FIG. 4. (a) Total thermal conductivity (κ_{total}) of $Ag_{1-x}M_xCrSe_2$ polycrystalline samples (M = Cu and Au; x = 0–0.03). The numbers in the parentheses indicate the relative density of the samples. (b) Electronic contribution to the thermal conductivity (κ_{el}) obtained using electrical resistivity shown in Fig. S8(a) [25] and Lorenz number.

unstable, making the structure easier to transition to the high-temperature phase where the Ag ions are in the disordered state. Additionally, the transition temperature decreases with both Cu substitution and Au substitution. This fact suggests that the structural phase transition in this system is dominated not by the size of the ions occupying the Ag site, but by the degree of disorder at the Ag site. In the Au-substituted samples, the decrease in T_{od} is more than 20 K, whereas the decrease in T_{od} in the Cu-substituted samples is smaller, around 10 K. It is believed that the Au substitution makes the structure more unstable and easier to transform to the high-temperature phase than the Cu substitution because Au tends to form bonds less easily with surrounding Se atoms compared to Cu.

Temperature dependence of total thermal conductivity (κ_{total}) is displayed in Fig. 4(a). The numbers in parentheses indicate the relative density of the samples used for the measurement. Open black circles represent the κ_{total} of pristine $AgCrSe_2$. It has been known that the relative density affects the value of thermal conductivity. Fig. S6(a) [25] compares the κ_{total} measured for samples with different relative densities. As shown in Fig. S6(a), a small difference in the relative density does not affect the thermal conductivity at low temperatures below ∼50 K, although it affects the values at high temperatures. Additionally, as shown in Fig. S6(b), the reproducibility of the data has been confirmed using samples with the same composition and density. These results mean that, at temperatures below 50 K, it is possible to discuss the trends among these samples. The magnitude of κ_{total} for $x = 0$ shown in Fig. 4(a) agrees well with the reported values [10] measured for the polycrystalline samples that were prepared using a sintering method similar to this study.

In Fig. 4(a), as the Cu-substitution level x increases, the κ_{total} systematically increases. In contrast, the κ_{total} systematically decreases as the Au-substitution level x increases. No systematic change is observed in the high-temperature region above 100 K, as shown in Fig. S7 [25], which is probably due to the difference in the relative density between the samples. The electronic contribution to the thermal conductivity (κ_{el}) is evaluated by using electrical resistivity shown in Fig. S8(a) [25] and the Lorenz number, $L = 2.45 \times 10^{-8}$ [W Ω K^{-2}]. The obtained values of κ_{el} are shown in Fig. 4(b). They are low enough in all the samples that the κ_{total} shown in Fig. 4(a) can be assumed to have a negligibly small electronic contribution. The lattice contribution (κ_{lat}) obtained by subtracting κ_{el} from κ_{total} is displayed in Fig. S8(b).

The in-plane electrical resistivity (ρ_{ab}) of $AgCrSe_2$ single crystals has been reported to be 9 mΩ cm at 300 K [26]. Although there is no report in the out-of-plane electrical resistivity (ρ_c) for $AgCrSe_2$, the electrical resistivity of this system has been known to be highly anisotropic; the value of ρ_c is three orders of magnitude greater than that of ρ_{ab} in the sulfur system, $AgCrS_2$ [26]. In polycrystalline samples, the values of electrical resistivity generally include both the in-plane and out-of-plane components. Indeed, the $x = 0$ sample shown in Fig. S8(a) exhibits the expected values as the order of magnitude intermediate between the in-plane and out-of-plane values.

As shown in Fig. S8(a), the values of electrical resistivity of the Au-substituted sample is almost the same as that of $x = 0$. On the other hand, the values of electrical resistivity of the Cu-substituted sample is one order of magnitude greater than those obtained for $x = 0$. The reason for this significant increase in the electrical resistivity by the Cu substitution can be explained as follows. First, since the Seebeck coefficient is positive across all temperature ranges [10], the electrical conduction carriers are holes. According to the electronic state calculations [30], $AgCrSe_2$ has bands composed of Cr and Se near the Fermi level. However, the density of states at the Fermi level is very small, suggesting the presence of small hole pockets. Given that the amount of the Cu substitution is only a few percent, the rigid band model can be applied, assuming that the band shape does not change with the Au or Cu substitution. Additionally, Ag and Au can be considered to be monovalent in $AgCrSe_2$. However, Cu generally prefers a divalent state rather than monovalent. Therefore, Cu substitution acts as electron doping, and even a small amount of substitution significantly reduces the number of hole carriers, resulting in the large increase in the electrical resistivity.

As marked by an arrow in Fig. 4(a), all the samples exhibit a peak at ∼15 K, which is one of the characteristics generally observed in crystalline samples: in the kinetic formulation, lattice thermal conductivity ($\kappa_{\rm lat}$) is given by the product of lattice specific heat ($C_{\rm lat}$), average velocity of phonon (ν), and phonon mean free path (ℓ) as $\kappa_{\rm lat} = 1/3C_{\rm lat}\nu\ell = 1/3C_{\rm lat}\nu^2\tau$. Here, τ is the phonon lifetime. At the lowest temperatures, ℓ has a constant value, and thus the $\kappa_{\rm lat}$ behaves as T^3 dominated by the temperature dependence of $C_{\rm lat}$. As temperature increases, the number of phonons increases, which leads to $\kappa_{\rm lat} \propto \exp(\Theta/T)$, where Θ is a temperature on the order of Debye temperature [27]. As a result, $\kappa_{\rm lat}$ generally exhibits a peak at a temperature where the dominant temperature dependence changes. Because the atomic mass of Au is larger than that of Ag, the reduced κ in the Au-substituted samples might be intuitive; the heavy Au ions scatter phonons more effectively than the Ag ions in the pristine sample.

For a closer examination of this, we conducted specific heat measurements. Fig. 5(a) displays the specific heat (C) of $AgCrSe_2$ and $Ag_{0.97}M_{0.03}CrSe_2$ (M = Cu, Au) polycrystalline samples. The values on the longitudinal axis are the specific heat divided by temperature. Each C/T vs. T curve exhibits a λ-type peak at 52 K, as indicated by an arrow in Fig. 5(a). This anomaly is attributed to a magnetic ordering of Cr^{3+} spins [28, 29]. As shown in Fig. 5(b), the $T_{\rm N}$ remains unaffected with the Cu or Au substitution because the changes in the lattice constants are very small.

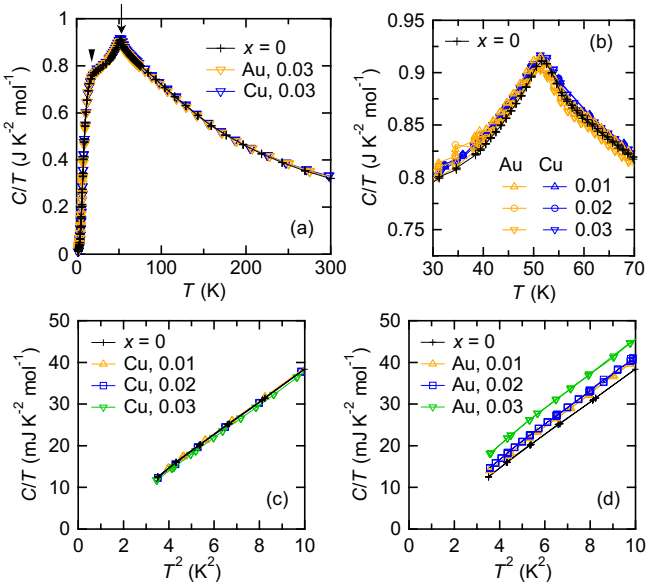

FIG. 5. (a) Specific heat of the samples. The anomaly at $T_{\rm N}$ = 52 K indicated by an arrow is attributed to a magnetic transition [15]. A large hump is also observed approximately at 20 K, as shown by a triangle, probably caused by the residual entropy due to disorder components of spin fluctuations. (b) Magnified view of the temperature region around the magnetic transition temperature. (c) and (d) display the C/T vs. T^2 plots of the specific heat of M = Cu and Au, respectively.

Notable feature is a hump observed around 20 K indicated by a triangle in Fig. 5(a). According to M. Baenitz *et al.* [30], there are several in-plane exchange interactions between Cr^{3+} ions. The nearest-neighbor interaction within the *ab*-plane is ferromagnetic, whereas the third-nearest-neighbor interaction is antiferromagnetic. The interaction between the planes is antiferromagnetic and significantly weaker compared to these interactions. Because of the magnetic frustration effect due to the competing exchange interactions between the two major interactions, Cr^{3+} has been known to form a cycloidal magnetic structure within the plane [30]. The observed hump might be from this cycloidal magnetic structure. The neutron diffraction [30] revealed that the magnitude of the ordered magnetic moment of Cr^{3+} at the lowest temperature is much smaller than the theoretical value predicted for $S = 3/2$. This fact suggests the presence of structural disorder or the existence of spin fluctuations persisting to very low temperatures. Therefore, the hump observed around 20 K might reflect the residual entropy

TABLE I. Structural parameters and anisotropic atomic displacement parameters U_{ij} (Å^2) for $AgCrSe_2$ and $Ag_{0.97}M_{0.03}CrSe_2$ (M = Cu and Au). The nominal compositions were used for the refinement.

$AgCrSe_2$, a = 3.68355(1) Å, c = 21.23955(6) Å, R_{wp} = 5.53%											
Atom	site	x	y	z	U_{iso}	U_{11}	U_{22}	U_{33}	U_{12}	U_{13}	U_{23}
Cr	3a	0	0	0.000(9)	0.0075(4)						
Se1	3a	0	0	0.269(9)	0.0042(4)						
Se2	3a	0	0	0.733(9)	0.0086(5)						
Ag	3a	0	0	0.153(8)	0.0604(12)	0.0841(13)	= U_{11}	0.0129(9)	= 1/2 U_{11}	0	0
$Ag_{0.97}Cu_{0.03}CrSe_2$, a = 3.68283(1) Å, c = 21.23655(6) Å, R_{wp} = 5.40%											
Atom	site	x	y	z	U_{iso}	U_{11}	U_{22}	U_{33}	U_{12}	U_{13}	U_{23}
Cr	3a	0	0	0.000(8)	0.0076(3)						
Se1	3a	0	0	0.269(8)	0.0067(4)						
Se2	3a	0	0	0.733(8)	0.0084(4)						
Ag/Cu	3a	0	0	0.152(8)	0.0568(10)	0.0738(11)	= U_{11}	0.0228(9)	= 1/2 U_{11}	0	0
$Ag_{0.97}Au_{0.03}CrSe_2$, a = 3.68327(2) Å, c = 21.24268(9) Å, R_{wp} = 4.96%											
Atom	site	x	y	z	U_{iso}	U_{11}	U_{22}	U_{33}	U_{12}	U_{13}	U_{23}
Cr	3a	0	0	0.000(9)	0.0067(4)						
Se1	3a	0	0	0.269(9)	0.0058(5)						
Se2	3a	0	0	0.733(9)	0.0071(5)						
Ag/Au	3a	0	0	0.152(9)	0.0618(12)	0.0908(14)	= U_{11}	0.0037(8)	= 1/2 U_{11}	0	0

of spins from the disorder components or spin fluctuations. Particularly, such humps are often observed in frustrated systems [31, 32].

Figs. 5(c) and 5(d) display the C/T of Cu- and Au-substituted samples, respectively, as a function of T^2. The values of C/T is almost unchanged by the Cu substitution, as shown in Fig. 5(c). On the contrary, the Au substitution increases the C/T. These results indicate that low-energy phonons, *i.e.*, the phonon DOS at low energies, increase in the Au-substituted $AgCrSe_2$. Because the increased number of phonons should scatter other phonons more frequently and reduce τ, the increase in C/T at low temperatures explains the reduced thermal conductivity of the Au-substituted $AgCrSe_2$. The T_N and the temperature at which the hump is observed remain unchanged by the Cu and Au substitutions. Therefore, the increase in C/T is attributed to the lattice contribution rather than the magnetic contribution.

To delve deeper into the reduced thermal conductivity in the Au-substituted samples, the Rietveld analysis was performed for the pristine, and $Ag_{0.97}M_{0.03}CrSe_2$ (M = Cu and Au) samples. Although a small amount of secondary phases has been observed in the profiles shown in Fig. 2(a), their quantity is minimal and does not affect the analysis. The nominal compositions are used for the refinement. All the fittings yielded low R_{wp} factors and reproduce well the experimentally obtained diffraction patterns, as shown in Figs. S9(a)–(c) [25].

Table I summarizes the refined structural parameters for the three samples. Anisotropic atomic displacement parameters, U_{ij}, are refined only for the Ag site because the refined values of the isotropic displacement parameters, U_{iso}, were found to be very small at the Cr and Se sites. The atomic positions show no significant differences among the three samples. On the other hand, the parameters U_{11} and U_{33} of the Ag site exhibit different values depending on the samples, which are plotted in Fig. 6 (a) in the order of M = Cu, Ag, and Au. Here, M = Ag represents the pristine $AgCrSe_2$.

As displayed in Fig. 6(a), U_{11} systematically increases, while U_{33} decreases, following the sequence of M = Cu, Ag, and Au. The variation of U_{11} and U_{33} is visualized in Figs. 6(b)–(d) using anisotropic displacement ellipsoids drawn at 80% probability level. Generally, atomic displacement parameters reflect the degree of static or dynamic disorder of the atoms. In this system, the Ag atoms exhibit the characteristic TA and LA modes with low energies vibrating within the *ab*-plane and along the c axis, respectively [6]. Therefore, the values of the obtained U_{11} and U_{33} mainly reflect the amplitude of the local atomic vibrations. As these localized vibration modes can effectively scatter other phonons, they are anticipated to reduce thermal conductivity. Additionally, larger vibration amplitudes would have greater scattering effects. Returning back to Fig. 4(a), the thermal conductivity systematically decreases with increasing Au substitution. Furthermore, U_{11} increases with Au substitution. Therefore, the increase in U_{11} is responsible for the reduced thermal conductivity in the Au-substituted samples.

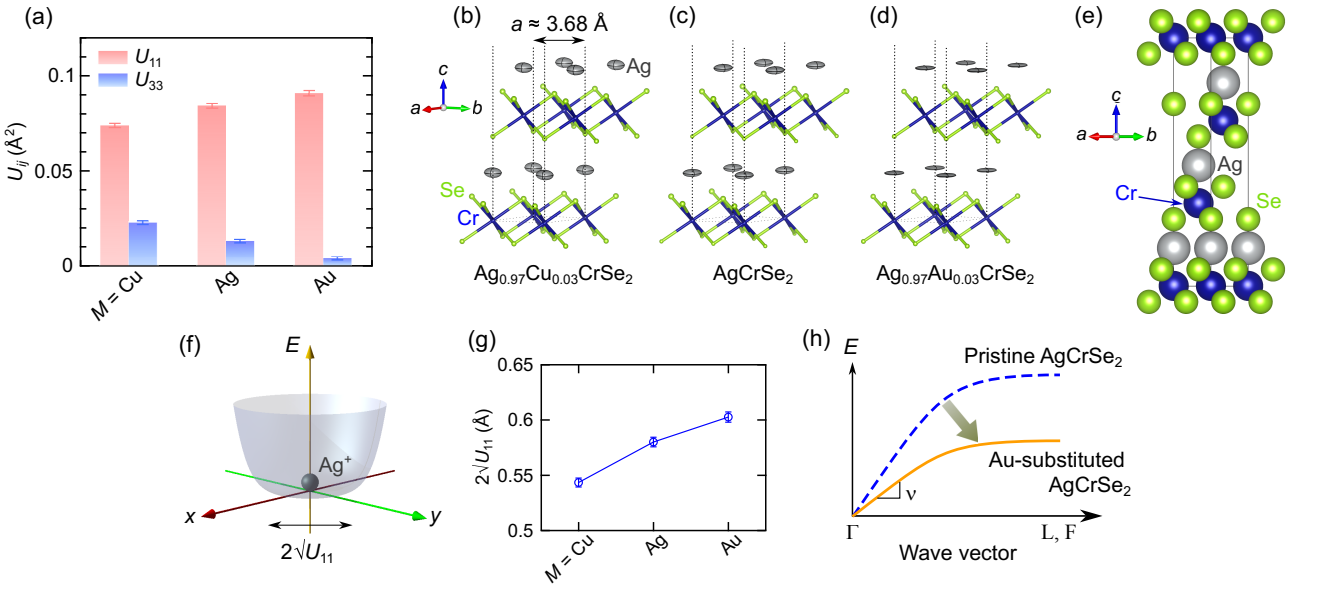

FIG. 6. (a) Anisotropic atomic displacement parameters U_{11} and U_{33} for $AgCrSe_2$ and $Ag_{0.97}M_{0.03}CrSe_2$ (M = Cu and Au) samples. M = Ag represents $AgCrSe_2$. (b), (c) and (d) display the crystal structures at room temperature of $Ag_{0.97}Cu_{0.03}CrSe_2$, $AgCrSe_2$, and $Ag_{0.97}Au_{0.03}CrSe_2$, respectively, with the anisotropic displacement ellipsoids drawn at 80% probability level for the Ag/Cu, Au atoms. (e) Crystal structure of $AgCrSe_2$ where the space filling is visualized using ionic radii. (f) Schematic image for a flat-bottomed potential well generated around each Ag ion. The value of $2\sqrt{U_{11}}$ is a measure of the width of the well indicated by a bothsided arrow. (g) The values of $2\sqrt{U_{11}}$ plotted for M = Cu, Ag, and Au. (h) Schematic diagram of the TA phonon dispersions. The curve of the pristine $AgCrSe_2$ refers to the results of the phonon calculation [6]. L and F represent the symmetry points at the first Brillouin zone boundary of the rhombohedral cell, and the wave vectors lie approximately within the Ag ion-conducting plane. ν in the formulation of $\kappa_{\rm lat} = 1/3C_{\rm lat}\nu\ell$ corresponds to the slope of the long-wavelength linear dispersion of the acoustic branch.

The composition dependent U_{11} and U_{33} indicate that the shape of the vibrational potential at the Ag site is altered by the Cu and Au substitutions. The ionic radii are in the order of Cu < Ag < Au, and the Ag site is surrounded by Se. The filling space for Ag ions along the c-axis is small, as shown in Fig. 6(e). On the other hand, there is larger space in the ab-plane, making the ions inherently easier to vibrate within the plane. Therefore, the change in the U_{11} and U_{33} due to the Cu and Au substitution can be explained as follows: The size of the ionic radius relative to the Ag ion significantly affects the ease of vibration along the c-axis direction, while the vibration amplitude is large within the ab-plane. As a result, the Au substitution suppresses the interplanar vibrations and enhances the in-plane vibrational amplitude, thereby modifying the potential energy landscape associated with the vibrations. Assuming a uniform distribution of the 3% substituent elements across the Ag plane, the average distance between them within the ab-plane is approximately 19 Å. There are only three unit cells apart along the [110] direction, and it is sufficient for the local modulation of the vibrational potential to significantly affect the overall vibrational state.

According to Raman scattering experiments [33], the localized low-energy vibrations in $AgCrSe_2$ are concluded as anharmonic vibrations which interact with higher optical modes to achieve low thermal conductivity. Fig. 6(f) depicts the schematic image for the anharmonic potential well at the Ag sites. Here, the square root of the U_{11} corresponds to the amplitude of the in-plane vibrations at the Ag sites. Therefore, the value of $\sqrt{U_{11}}$ multiplied by a factor of 2 is a measure of the width of the potential well indicated by the double-sided arrows in Fig. 6(f). Fig. 6(g) plots the values of $2\sqrt{U_{11}}$ for M = Cu, Ag, and Au. It increases in the order of M = Cu, Ag, and Au, reaching up to 16.4% of the Ag-Ag distance (= lattice constant a) for M = Au. These results indicate that the anharmonicity is enhanced by the Au substitution and contributes to the reduction of the lattice thermal conductivity through increased phonon-phonon scattering. The contribution of anharmonic vibrations to the reduction of thermal conductivity has also been observed in several compounds [34, 35].

The enhancement in the in-plane vibrational amplitude should also decrease the force constants between the adjacent Ag/Au ions, *i.e.*, decrease in the Ag-Ag bonding strength, which should cause softening of the TA branch, as shown in Fig. 6(h). The reduced slope of the TA mode indicates a lower phonon velocity, ν, which directly contributes to the reduction of lattice thermal conductivity, as $\kappa_{\rm lat} \propto \nu^2\tau$. Simultaneously, the number of low-energy phonons would increase, which explains the trend of C/T

shown in Fig. 4(c), and further contributes to the suppression of thermal transport.

Ultra-low thermal conductivity in ionic conductors has long remained a mystery in the field of thermoelectrics, and the relationship between atomic dynamics and thermal transport has not been clearly understood, as discussed in the Introduction. The main achievement of this study is not merely the observation of reduced thermal conductivity due to Au substitution, but rather identification of enhanced anharmonicity in the ion-conducting species as the underlying origin of the ultra-low thermal conductivity. This anharmonicity leads to an increased number of low-energy phonons, which further contributes to the suppression of thermal transport. These insights are broadly applicable to the thermal behavior not only of other superionic conductors, but also of compounds with fluctuating sublattices [36, 37], extending beyond the $AgCrSe_2$ system itself. In this context, the progress described in this study offers a solid foundation for advancing the use of ionic conductors in thermoelectric applications. We believe our results provide meaningful guidance for future strategies in lattice-related functional materials.

IV. CONCLUSIONS

Thermal conductivity, electrical resistivity, specific heat, and structural parameters have been characterized for $Ag_{1-x}M_xCrSe_2$ (M = Cu and Au). The Au substitution for the Ag site systematically decreases the thermal conductivity with increasing x. On the contrary, the Cu substitution enhances the thermal conductivity. Specific heat measurements reveal that Au substitution leads to an increase in the low-energy phonons. Powder x-ray structure refinement further demonstrates that Au substitution increases the in-plane atomic displacement parameter U_{11}. This clearly indicates an enhancement in the amplitude of in-plane vibrations of Ag atoms, which reflects increased anharmonicity in their vibrational potential. At the same time, the large vibrational amplitude also indicates a reduction in the force constants between Ag atoms, which results in a decrease in the phonon velocity of the corresponding acoustic mode. The increase in the low-energy phonons is likely caused by the reduction in these force constants. Both the increase in the low-energy phonons and the enhancement of in-plane vibrational amplitude contribute to a reduction in the phonon lifetime, and thus govern the ultra-low thermal conductivity of this system. This anharmonicity-based scenario is generally applicable to other superionic conductors, and we believe that our findings represent a solid step forward for future research on thermoelectric materials.

ACKNOWLEDGMENTS

The authors thank Dr. K. Osaka for his support to conduct the experiments at BL19B2. The synchrotron radiation experiments were performed at BL02B2 (Proposal No. 2022A2077) and BL19B2 of SPring-8. This work was partially supported by an SDGs Research Project of Shimane University. J.M. and J.F.Z. thank the financial support from the National Science Foundation of China (No. 12334008).

[1] D. W. Murphy, H. S. Chen and B. Tell, Superionic Conduction in $AgCrS_2$ and $AgCrSe_2$, *J. Electrochem. Soc.* **124**, 1268 (1977).

[2] B. A. Boukamp and G. A. Wiegers, Ionic and electronic processes in $AgCrSe_2$, *Solid State Ionics* **9-10**, 1193 (1983).

[3] H. Liu, X. Shi, F. Xu, L. Zhang, W. Zhang, L. Chen, Q. Li, C. Uher, T. Day, and G. J. Snyder, Copper ion liquid-like thermoelectrics, *Nature Mater.* **11**, 422 (2012).

[4] Q. Ren, M. K. Gupta, M. Jin, J. Ding, J. Wu, Z. Chen, S. Lin, O. Fabelo, J. A. R.-Velamazán, M. Kofu *et al.*, Extreme phonon anharmonicity underpins superionic diffusion and ultralow thermal conductivity in argyrodite Ag_8SnSe_6, *Nature Mater.* **22**, 999 (2022).

[5] D. J. Voneshen, H. C. Walker, K. Refson, and J. P. Goff, Hopping Time Scales and the Phonon-Liquid Electron-Crystal Picture in Thermoelectric Copper Selenide, *Phys. Rev. Lett.* **118**, 145901 (2017).

[6] J. Ding, J. L. Niedziela, D. Bansal, J. Wang, X. He, A. F. May, G. Ehlers, D. L. Abernathy, A. Said, A. Alatas *et al.*, Anharmonic lattice dynamics and superionic transition in $AgCrSe_2$, *Proc. Natl. Acad. Sci. U.S.A.* **117**, 3930 (2020).

[7] L. Xie, J. H. Feng, R. Li, and J. Q. He, First-Principles Study of Anharmonic Lattice Dynamics in Low Thermal Conductivity $AgCrSe_2$: Evidence for a Large Resonant Four-Phonon Scattering, *Phys. Rev. Lett.* **125**, 245901 (2020).

[8] J. Ding, T. L.-Atkins, M. C.-Cueva, A. Banerjee, D. L. Abernathy, A. Said, A. Zevalkink, O. Delaire, Soft anharmonic phonons and ultralow thermal conductivity in $Mg_3(Sb, Bi)_2$ thermoelectrics, *Sci. Adv.* **7**, 1449 (2021).

[9] C. Wang and Y. Chen, Highly selective phonon diffusive scattering in superionic layered $AgCrSe_2$, *Comput. Mater.* **6**, 26 (2020).

[10] F. Damay, S. Petit, S. Rols, M. Braendlein, R. Daou, E. Elkaïm, F. Fauth, F. Gascoin, C. Martin, and A. Maignan, Localised Ag^+ vibrations at the origin of ultralow thermal conductivity in layered thermoelectric $AgCrSe_2$, *Sci. Rep.* **6**, 23415 (2016).

[11] F. Gascoin and A. Maignan, Order-Disorder Transition in $AgCrSe_2$: a New Route to Efficient Thermoelectrics, *Chem. Mater.* **23**, 2510 (2011).

[12] S. Bhattacharya, A. Bohra, R. Basu, R. Bhatt, S. Ahmad, K. N. Meshram, A. K. Debnath, A. Singh, S. K. Sarkar, M. Navneethan *et al.*, High thermoelectric per-

formance of $(AgCrSe_2)_{0.5}(CuCrSe_2)_{0.5}$ nano-composites having all-scale natural hierarchical architectures, *J. Mater. Chem. A* **2**, 17122 (2014).

[13] D. Wu, S. Huang, D. Feng, B. Li, Y. Chen, J. Zhang, and J. He, Revisiting $AgCrSe_2$ as a promising thermoelectric material, *Phys. Chem. Chem. Phys.* **18**, 23872 (2016).

[14] S. Bhattacharya, R. Basu, R. Bhatt, S. Pitale, A. Singh, D. K. Aswal, S. K. Gupta, M. Navaneethan, and Y. Hayakawa, $CuCrSe_2$: a high performance phonon glass and electron crystal thermoelectric material, *J. Mater. Chem. A* **1**, 11289 (2013).

[15] F. M. R. Engelsman , G. A. Wiegers, F. Jellinek, and B van Laar, Crystal Structures and Magnetic Structures of Some Metal(I) Chrominm(III) Sulfides and Selenides, *J. Solid State Chem.* **6**, 574 (1973).

[16] A. Van Der Lee , G. A. Wiegers, Anharmonic Thermal Motion of Ag in $AgCrSe_2$: A High-Temperature Single-Crystal X-Ray Diffraction Study, *J. Solid State Chem.* **82**, 216 (1989).

[17] A. Gagor, D. Gnida, A. Pietraszko, Order-disorder phenomena in layered $CuCrSe_2$ crystals, *Mater. Chem. Phys.* **146**, 283 (2014).

[18] J. L. Niedziela, D. Bansal, A. F. May, J. Ding, T. L.-Atkins, G. Ehlers, D. L. Abernathy, A. Said, and O. Delaire, Selective breakdown of phonon quasiparticles across superionic transition in $CuCrSe_2$, *Nature Phys.* **15**, 73 (2019).

[19] A. Maignan, E. Guilmeau, F. Gascoin, Y. Bréard, and V. Hardy, Revisiting some chalcogenides for thermoelectricity, *Sci. Technol. Adv. Mater.* **13**, 053003 (2012).

[20] B. Li, H. Wang, Y. Kawakita, Q. Zhang, M. Feygenson, H. L. Yu, D. Wu, K. Ohara, T. Kikuchi, K. Shibata *et al.*, Liquid-like thermal conduction in intercalated layered crystalline solids, *Nature Mater.* **17**, 226 (2018).

[21] K. Momma, and F. Izumi, VESTA3 for three-dimensional visualization of crystal, volumetric and morphology data, *J. Appl. Crystallogr.* **44**, 1272 (2011).

[22] M. S. Whittingham, Chemistry of intercalation compounds: Metal guests in chalcogenide hosts, *Prog. Solid State Chem.* **12**, 41 (1978).

[23] A. G. Gerards, B. A. Boukamp, and G. A. Wiegers, Neutron diffraction study of the order-disorder transition in $AgCrS_2$, *Solid State Ionics* **9–10**, 471 (1983).

[24] F. Damay, C. Martin, V. Hardy, G. André, S. Petit, and A. Maignan, Magnetoelastic coupling and unconventional magnetic ordering in the multiferroic triangular lattice $AgCrS_2$, *Phys. Rev. B* **83**, 184413 (2011).

[25] See Supplemental Material for additional information for (i) powder x-ray diffraction experiment, (ii) DSC measurement, (iii) thermal conductivity, and (iv) structural refinement using synchrotron diffraction data.

[26] R. Yano and T. Sasagawa, Crystal Growth and Intrinsic Properties of $ACrX_2$ (A = Cu, Ag; X = S, Se) without a Secondary Phase,

[27] N. W. Ashcroft and N. D. Mermin, *Solid State Physics*; Thomson Learning, Inc.: USA, 1976. *Cryst. Growth Des.* **16**, 5618 (2016).

[28] P. Bongers, C. F. Van Bruggen, J. Koopstra, W. P. F. A. M. Omloo, G. A. Wiegers, and F. Jellinek, Structures and magnetic properties of some metal (I) chromium (III) sulfides and selenides, *J. Phys. Chem. Solids* **29**, 977 (1968).

[29] U. K. Gautam, R. Seshadri, S. Vasudevan, and A. Maignan, Magnetic and transport properties, and electronic structure of the layered chalcogenide $AgCrSe_2$. *Solid State Commun.* **2002**, *122*, 607-612, *Solid State Commun.* **122**, 607 (2002).

[30] M. Baenitz, M. M. Piva, S. Luther, J. Sichelschmidt, K. M. Ranjith, H. D.-Dębicki, M. O. Ajeesh, S.-J. Kim, G. Siemann, C. Bigi *et al.*, Planar triangular magnet: Magnetic frustration, short range correlations, and field-tuned anisotropic cycloidal magnetic order, *Phys. Rev. B* **104**, 134410 (2021).

[31] T. Okuda, Y. Beppu, Y. Fujii, T. Onoe, N. Terada, and S. Miyasaka, Specific heat of delafossite oxide $CuCr_{1-x}Mg_xO_2$ ($0 \leq x \leq 0.03$), *Phys. Rev. B* **77**, 134423 (2008).

[32] H. Takatsu, H. Yoshizawa, S. Yonezawa, and Y. Maeno, *Phys. Rev. B* **79**, 104424 (2009).

[33] K. S. Rana, A. Singh, A. Bhui, K. Biswas, and A. Soni, Anharmonic Phonon Vibrations of Ag and Cu for Poor Lattice Thermal Conductivity in Superionic $AgCrSe_2$ and $CuCrSe_2$, *ACS Appl. Energy Mater.* **7**, 5621 (2024).

[34] B. C. Sales, D. Mandrus, and R. K. Williams, Filled Skutterudite Antimonides: A New Class of Thermoelectric Materials, *Science* **272**, 1325 (1996).

[35] Y. Zhang, V. Ozoliņš, D. Morelli, and C. Wolverton, Prediction of New Stable Compounds and Promising Thermoelectrics in the Cu-Sb-Se System, *Chem. Mater.* **26**, 3427 (2014).

[36] J. Zhang, N. Roth, K. Tolborg, S. Takahashi, L. Song, M. Bondesgaard, E. Nishibori, and B. B. Iversen, Direct observation of one-dimensional disordered diffusion channel in a chain-like thermoelectric with ultralow thermal conductivity, *Nat. Commun.* **12**, 6709 (2021).

[37] M. K. Jana, K. Pal, A. Warankar, P. Mandal, U. V. Waghmare, K. Biswas, Intrinsic Rattler-Induced Low Thermal Conductivity in Zintl Type $TlInTe_2$, *J. Am. Chem. Soc.* **139**, 4350 (2017).